Biosensors and Bioelectronics 157 (2020) 112167

Contents lists available at ScienceDirect

Biosensors and Bioelectronics

journal homepage: http://www.elsevier.com/locate/bios

Monitoring the hemostasis process through the electrical characteristics of a graphene-based field-effect transistor

Ariadna Schuck [a,b], Hyo Eun Kim [a], Kyung-Mo Jung [a], Willyan Hasenkamp [b], Yong-Sang Kim [a,*]

[a] Department of Electrical and Computer Engineering, Sungkyunkwan University, Suwon, Republic of Korea
[b] Electrical Engineering Graduate Program and itt CHIP - Semiconductor Institute, Universidade do Vale do Rio dos Sinos, São Leopoldo, Brazil

ARTICLE INFO

Keywords:
Graphene
Field-effect transistor
Hemostasis
Biosensor

ABSTRACT

Graphene-based transistors are promising devices in the evaluation of carrier density in biological analytes. We report on the design and fabrication of a graphene-based field-effect transistor for monitoring and assessing the interaction between the coagulation factors based on the charge carrier density in a blood sample. When biochemical reactions occurred during the coagulation cascade process, a dopant effect was noticed on the graphene surface by the change in Dirac point voltage values. Additional experiments were performed using blood samples treated with activators (vitamin K, calcium chloride, and thromboplastin reagent) and inhibitors (heparin drugs) to evaluate the selectivity of the graphene field-effect transistor devices. Since the transfer characteristic curves presented divergent behaviours for different levels of procoagulants and anticoagulants, the measurements showed that the devices can assess changes in the concentrations of factors that inhibit or accelerate the cascade process when using untreated and treated samples. Reproducibility was verified by testing samples from different sources. To the best of our knowledge, this study is the first to demonstrate the potential of graphene in monitoring the hemostasis process through the analysis of the electrical properties of human whole blood.

1. Introduction

Hemostasis is an important and complex physiological process that initiates after vascular trauma to prevent blood loss (Lei et al., 2013; Palta et al., 2014; Wahed and Dasgupta, 2015; Winter et al., 2017). This multi-factorial biological mechanism is essential to maintain optimal blood rheology and can be used to detect and control many disorders that affect the clotting time of the patient, thus avoiding serious pathological complications in the vascular system, such as hemorrhage, venous thrombosis, and embolism (Bazaev et al., 2015; Chapin and Hajjar, 2015; Palta et al., 2014; Ramaswamy et al., 2013). Within a few seconds after the trauma, the primary stage of hemostasis starts with vascular constriction and platelet plug formation (Wahed and Dasgupta, 2015; Winter et al., 2017). This is followed by the secondary stage known as coagulation cascade, wherein fibrin clot formation and the growth of fibrous tissue occur (Bazaev et al., 2015; Lei et al., 2013; Wahed and Dasgupta, 2015; Winter et al., 2017). The cascade process can be activated by the intrinsic pathway (contact) or by the extrinsic pathway (tissue factor) according to the *in vitro* analysis model (Winter et al., 2017). The coagulation process involves many biological components that can be classified as procoagulants (e.g., fibrinogen (factor I)) which promote clot formation, and anticoagulants (e.g., antithrombin (AT)) which inhibit biochemical reactions (Bazaev et al., 2015; Lane, 2005; Palta et al., 2014; Tormoen et al., 2013). Most tests for coagulation, such as prothrombin time (PT) and activated partial thromboplastin time (aPTT) measurements, are recorded by automated coagulation analyzers using photo-optical or electromechanical methods (Bazaev et al., 2015; Harris et al., 2013; Yang, 2013). Fibrin formation can be determined by changes in the mechanical and electrical properties of blood or through ultrasonic/optical measurements (Bazaev et al., 2015; Cakmak et al., 2014; Lei et al., 2013; Maji et al., 2017).

Biosensor devices for point-of-care diagnostics have several advantages, such as miniaturization, integration, accuracy, and automation of biological and chemical testing (Ramaswamy et al., 2013; Tzong-Jih Cheng et al., 1998; Yang, 2013). These also provide a well-controlled environment for the investigation of biological processes, such as coagulation (Lei et al., 2013; Ramaswamy et al., 2013; Tzong-Jih Cheng et al., 1998; Yang, 2013). Some point-of-care devices for the determination of blood coagulation time have been reported, with most based

* Corresponding author. Engineering Building, 1 (23), Room 23232, 2066, Seobu-ro Jangan-gu, Suwon, Gyeonggi-do, Republic of Korea.
E-mail address: yongsang@skku.edu (Y.-S. Kim).

https://doi.org/10.1016/j.bios.2020.112167
Received 12 December 2019; Received in revised form 5 February 2020; Accepted 20 March 2020
Available online 22 March 2020

on detecting changes in the mechanical and optical properties of blood using piezoelectric quartz crystals and optical methods (Harris et al., 2013; Müller et al., 2010; Tzong-Jih Cheng et al., 1998; Yang, 2013; Yao et al., 2013). However, only a few studies have evaluated coagulation time by investigating the electrical properties of blood using, for example, electrochemical impedance or dielectric spectroscopy sensors (Harris et al., 2013; Lei et al., 2013; Maji et al., 2017, 2015; Ramaswamy et al., 2013).

Graphene is a nanocarbon material that presents unique electronic properties, and a large surface area (Andronescu and Schuhmann, 2017; Lei et al., 2017; Mao and Chen, 2017; Forsyth et al., 2017). It is emerging as one of the most promising biocompatible nanomaterials for use in point-of-care biomedical applications (Dong et al., 2010; Han et al., 2017; Mao and Chen, 2017; Forsyth et al., 2017; Suvarnaphaet and Pechprasarn, 2017). Additionally, graphene has the potential for use in a low-cost biosensor with high sensitivity and specificity (Andronescu and Schuhmann, 2017; Forsyth et al., 2017; Suvarnaphaet and Pechprasarn, 2017). In the last decade, the graphene field-effect transistor (GFET) has been studied for application as a sensor to detect biomolecules such as DNA, RNA, proteins, and enzymes (Andronescu and Schuhmann, 2017; Dong et al., 2010; Han et al., 2017; Kim et al., 2019; Lei et al., 2017; Mao and Chen, 2017; Forsyth et al., 2017; Suvarnaphaet and Pechprasarn, 2017). GFET sensing uses the electrical response detected upon the binding or adsorption of charged biomolecules to the graphene surface through π-π stacking interactions while an electric field is applied to the gate terminal (Fu et al., 2017; Han et al., 2017; Kim et al., 2019; Forsyth et al., 2017; Tran and Mulchandani, 2016). The neutrality point, also known as the Dirac point, is a material property that defines the doping effect on the graphene (Dong et al., 2010; Fu et al., 2017; Han et al., 2017; Suvarnaphaet and Pechprasarn, 2017; Tran and Mulchandani, 2016). An additional benefit is that it is easier to control the doping concentration and improve mobility in a graphene-based field-effect transistor as compared to other devices (Dong et al., 2010; Han et al., 2017; Kim et al., 2019; Kwak et al., 2012).

In this work, we designed and fabricated a solution-gate graphene-based field-effect transistor. The GFET device was used to investigate interactions between a non-functionalized graphene layer and whole blood samples throughout the hemostasis process. Blood samples were also treated with different volumes of activators (vitamin K, calcium chloride, and thromboplastin reagent) and inhibitors (heparin drugs) to evaluate the selectivity of the device and the effects of these biochemical components in the coagulation cascade. Lastly, reproducibility was verified using different blood samples.

2. Material and methods

2.1. Materials

AZ-1512, SU-8 2075, hexamethyldisilazane (HMDS) and (1-methoxy-2-propyl) acetate (SU-8 developer) were obtained from MicroChem Corp. (Westborough, U.S.A.). Polydimethylsiloxane (Sylgard 184 A/B) was purchased from Dow Corning (Seoul, Korea). Graphene layer grown by CVD was acquired from Graphenea (San Sebastián, Spain). Calcium chloride, vitamin K_1, enoxaparin sodium, parnaparin sodium, iron (III) chloride powder, and phosphate-buffered saline were supplied by Sigma-Aldrich Corp. (St. Louis, U.S.A.). Thromborel S Reagent was purchased from Sysmex Korea Co., Ltd. (Seoul, Korea). Trisodium citrate tube (1.8 mL) is courtesy of AB Medical, Inc. (Nam-myeon, Korea). Illustrations were created with BioRender.

2.2. Fabrication of solution-gate GFET devices

Three coplanar terminals (source, drain, and gate) were deposited on the substrate using photolithography coupled with metal deposition by thermal evaporation (Han et al., 2017; Kim et al., 2019). To fabricate the terminals, glass substrates were first cleaned by ultrasonication in acetone, then in isopropyl alcohol (IPA) for 10 min each. After drying, the glass surface was first spin-coated with HMDS to promote adhesion, and then with AZ-1512 positive photoresist (PR) (Fig. S1A). Substrates were soft baked for 10 min at 95 °C in a conventional oven. To pattern the terminals using a photomask, the glasses were exposed to ultraviolet (UV) radiation by a mask aligner (MA-6, Karl-Suss) (Fig. S1B). After dissolving the exposed PR (Fig. S1C), a titanium (Ti) layer was deposited over the glass as a support layer using a vacuum thermal evaporator (Evaporation System SHE-6T-350D), followed by deposition of a gold (Au) layer (Fig. S1D). To remove the residual photoresist, the substrates were placed in an acetone bath, ultra-sonicated, then dried.

Next, CVD-grown graphene (5×5 mm^2) was spin-coated with a triple-layer of PDMS (mixing base and curing agents of silicone elastomer in 9:1 v/v ratio) and cured for 10 min at 95 °C after the deposition of each layer (Fig. S1E). Copper was etched away from the PDMS/graphene/Cu film using ferric chloride solution ($FeCl_3$, 0.25 mg/mL) for 15 min at room temperature (Fig. S1F). The layer was rinsed with DI water and then transferred onto the region between the source and drain terminals using DI water as a transfer medium and with the support of tweezers (Fig. S1G). The PDMS/graphene top surface was blow-dried with a nitrogen gun for a few seconds to reduce the water concentration under the film, and the substrate was placed for 5 min in an oven at 75 °C. The PDMS layer was removed from the graphene layer after placing the device in an acetone bath for 1 h. The substrate was cleaned with IPA and DI water, then dried with nitrogen.

To deliver the biological sample that interacts with the non-functionalized graphene surface, a PDMS microfluidic channel was fabricated on top of the region between the active layer and the gate terminal. The channel mold was also fabricated using a photolithography technique in which a silicon wafer (4 inches) was spin-coated with negative photoresist (SU-8 2075), exposed to UV radiation, then soft-baked in an oven for 5 min at 65 °C, followed by 12 more minutes at 95 °C. The silicon wafer was immersed in SU-8 developer ((1-methoxy-2-propyl) acetate) for 5 min and rinsed with IPA and DI water. Then, the wafer was hard-baked in an oven for 30 min at 150 °C. Base and curing agents (10:1 v/v ratio) of silicone elastomer were mixed and poured onto the mold (Fig. S1H). After degassing at room temperature, PDMS was cured for 1 h at 75 °C. The polymer was peeled off, then cut and drilled to allow access to the microchannel through the inlet and outlet holes. The microfluidic channel was cleaned with IPA and DI water, then bonded onto the glass substrate by an UV-ozone treatment (Fig. S1I). The device has the configuration of a solution-gate GFET fabricated on a glass substrate integrated with a polydimethylsiloxane (PDMS) microfluidic channel (Fig. 1).

2.3. Measurement and characterization

In this study, transfer curve measurements were carried out using an HP Agilent 4145B Semiconductor Parameter Analyzer coupled with a probe station. To evaluate device performance and create a reference point, phosphate-buffered saline (PBS) solution was injected into the channel. The drain current (I_D) was measured while applying different bias voltages (V_G) to the common gate terminal while keeping the drain voltage (V_D) constant at 0.4 V. For the experiments carried out using biological samples, the transfer curves were measured repeatedly for 15 min at an interval of 30 s. Then, the Dirac point and drain current could be evaluated for each device over the course of the experiment. The measured electrical signals indicate a doping effect occurred during the biological process, the increase or decrease in charge density over the active layer surface result in a left- or right-shift of the Dirac point (Dong et al., 2010; Han et al., 2017).

2.4. Sample preparation

To perform the clotting test, whole human blood sample kept in 3.2%

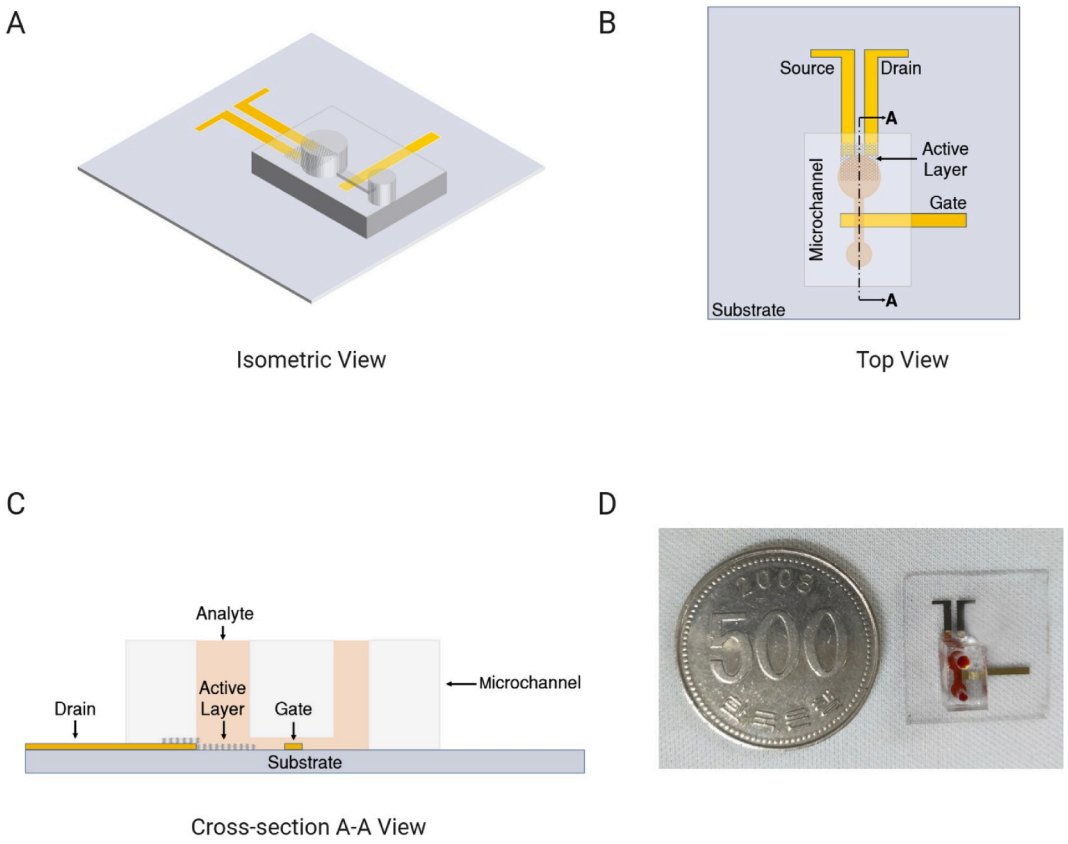

Fig. 1. Microchannel integrated with a solution-gate graphene-based field-effect transistor to monitor the electrical properties of the hemostasis process. (A) Isometric view. (B) Top view. (C) Cross-sectional A-A view. (D) GFET device prototype.

sodium citrate anticoagulant collection tubes at 37 °C were used. After device characterization, the PBS solution was removed from the microchannels, and the pathways were cleaned with IPA/DI water and then dried in an oven at 75 °C for 5 min. To initiate coagulation in the whole blood supplemented with anticoagulant, calcium chloride ($CaCl_2$) was added in the sample to initiate clotting before injecting 10 μL of whole blood (Fig. 2A) into the channel (Lei et al., 2013; Maji et al., 2017, 2015). Subsequently, measurements were performed to obtain the I_D-V_G response curves as described herein (Fig. 2B–C). Additionally, blood samples were treated with several biochemicals (Table S1) to alter the clotting process by activating or restricting certain blood factors after the onset of hemostasis. Vitamin K (Vit_K), thromboplastin reagent (TR) and calcium ions ($CaCl_2$) were chosen as activators. To inhibit the process, heparin drugs were selected based on the different ratios of anti-Xa to anti-IIa activity.

2.5. Data analysis and statistics

Data analysis was performed in Origin 8.5.0, including the normalization process. Also, the medians, means and standard deviation values were calculated using Origin 8.5.0.

3. Results

3.1. Effect of the hemostasis process on the graphene surface

The electrical properties of the sensors were characterized using PBS solution to obtain a reference point. After measuring the transfer characteristic curves of the GFET devices (Fig. S2A), a mean Dirac point voltage (V_{Dirac}) of 0.99 V (n = 40; median of 1 V; standard deviation (SD) of ±0.02 V) (Fig. S2B) was obtained. The GFET devices were stored in a dry box at room temperature and for one week the stability of the devices were verified using the buffer solution. The average value of the Dirac point voltages was 1.02 V (SD of ±0.03 V; n = 10) presenting a small variation when compared with the value measured (0.99 V) right after the device was produced. All microchannels were cleaned with deionized (DI) water and dried before the biological experiment. After sample incubation and re-calcification, 10 μL of human whole blood (HWB) was injected into the channel. The drain current (I_D)-gate voltage (V_G) characteristic curve was recorded during primary (Fig. 3A) and secondary (Fig. 3B) hemostasis caused by the vessel injury. Using the mean V_{Dirac} value of PBS solution as a reference point, a shift of 0.53 V towards lower V_G values was observed after the injection of blood (Fig. 3C). The curve response indicates that there was an increase in negative charge density over the graphene surface during the coagulation cascade (Dong et al., 2010; Kwak et al., 2012; Levesque et al., 2011). This phenomenon is observed because of the exposure of platelet phospholipids (PL) during the first step of the hemostasis process (Fig. 3A). These negatively charged lipids, which are located in the activated platelet membrane, bind with plasma protein molecules (factor V and factor X) through calcium ions (BERMINGHAM et al., 1968; BHAGAVAN, 2002; Boon, 1993; Morin, 1980; Periayah et al., 2017). Additionally, there exists increased carrier concentration due to the activation of anti- and procoagulants in the coagulation cascade (Boon, 1993; Palta et al., 2014; Sperling et al., 2017). The experiments were repeated in two additional devices using aliquots of the same sample, and a shift in V_{Dirac} between 0.8 V and 0.6 V was observed (Fig. 3D). High-magnification images show the clot that formed on the graphene surface (Fig. 3E) after being transferred to a glass substrate. The red blood cells that were not included in the cross-linked fibrin can be seen.

To evaluate clot formation in altered blood samples and to optimize device selectivity, further experiments were carried out using samples treated with different volumes of biochemical components that affect the hemostasis process. To accelerate the reactions of the coagulation

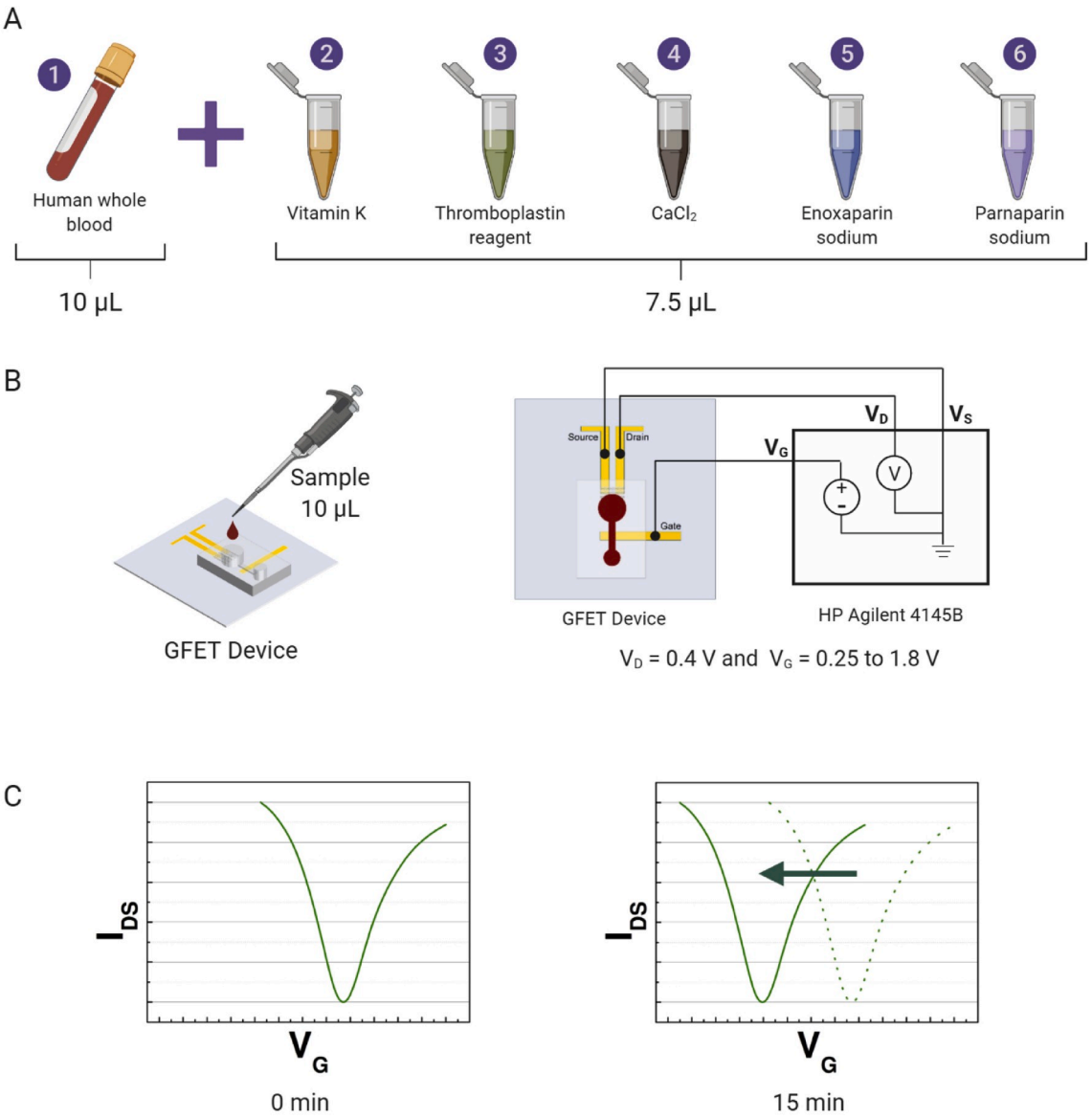

Fig. 2. Schematic representation of the GFET sensor experiments using different analytes. (A) Pristine human whole blood samples were prepared and mixed with activators (vitamin K, thromboplastin reagent, and $CaCl_2$) and inhibitors (enoxaparin sodium and parnaparin sodium). (B) Sample injection into the channel and measurement setup using a semiconductor parameter analyzer. (C) Behavior of the transfer characteristic curves during testing of the biological samples.

cascade, the blood was treated with different activators, vitamin K, thromboplastin reagent and $CaCl_2$ (Golder et al., 2013; Palta et al., 2014; Periayah et al., 2017). And to restrain the hemostasis process, two types of negatively charged low-molecular-weight heparin (LMWH) drugs were added to the whole blood samples to act as a thrombin inhibitor (Funk, 2012; Merli and Groce, 2010; Palta et al., 2014; Tripodi, 2016). The anticoagulant drugs, enoxaparin sodium ($LMWH_E$) and parnaparin sodium ($LMWH_P$), were selected for these experiments. Both types of heparin directly inhibit factor X after its activation, but the effects of the different types of LMWH on each factor that participates in the clot formation process are still unclear (Wahed and Dasgupta, 2015; White and Ginsberg, 2003). Therefore, it is understandable that divergent behaviours are observed when monitoring the hemostasis process using heparin-treated samples because the ratios of anti-factor Xa and anti-thrombin activities vary with heparin type (Schoen et al., 1992; White and Ginsberg, 2003).

First, the transfer curves (Fig. S3) were measured for each device containing different volumes (2.5, 5.0, 7.5 µL) of activators and inhibitors in the total analyte volume. Then, to guarantee the effect of each biochemical in the main experiment, a volume of 7.5 µL of each biochemical was defined to be used in the GFET devices and the Dirac point voltage values were obtained (Fig. 4A) based on the measured transfer curves (Fig. S3). Afterward, each component (7.5 µL) was added to the blood drawn (10 µL) and an aliquot of 10 µL was injected into the channel. The changes in the neutrality point values (V_{Dirac}) of the different devices based on the initial transfer curves (Fig. S4) measured during the coagulation cascade can be observed considering the values of the Dirac point (Fig. 4B). The median values and the standard deviations of the activators and inhibitors before and after adding the blood samples are presented in Table S2. Decreased V_{Dirac} values were seen in all devices immediately after the injection of the samples (untreated and treated blood samples) into the microchannels. Vitamin K (Fig. 4C) stimulates the cascade process while increasing specific factors in the sample, thus providing a smaller Dirac point voltage value. Tissue factor triggers the extrinsic pathway (Fig. 3B), also promoting faster clot formation than in the other samples, which is reflected in the V_{Dirac} value of the sample treated with TR. Calcium chloride increases protein-phospholipid interactions (Fig. 4D), thereby accelerating clot formation

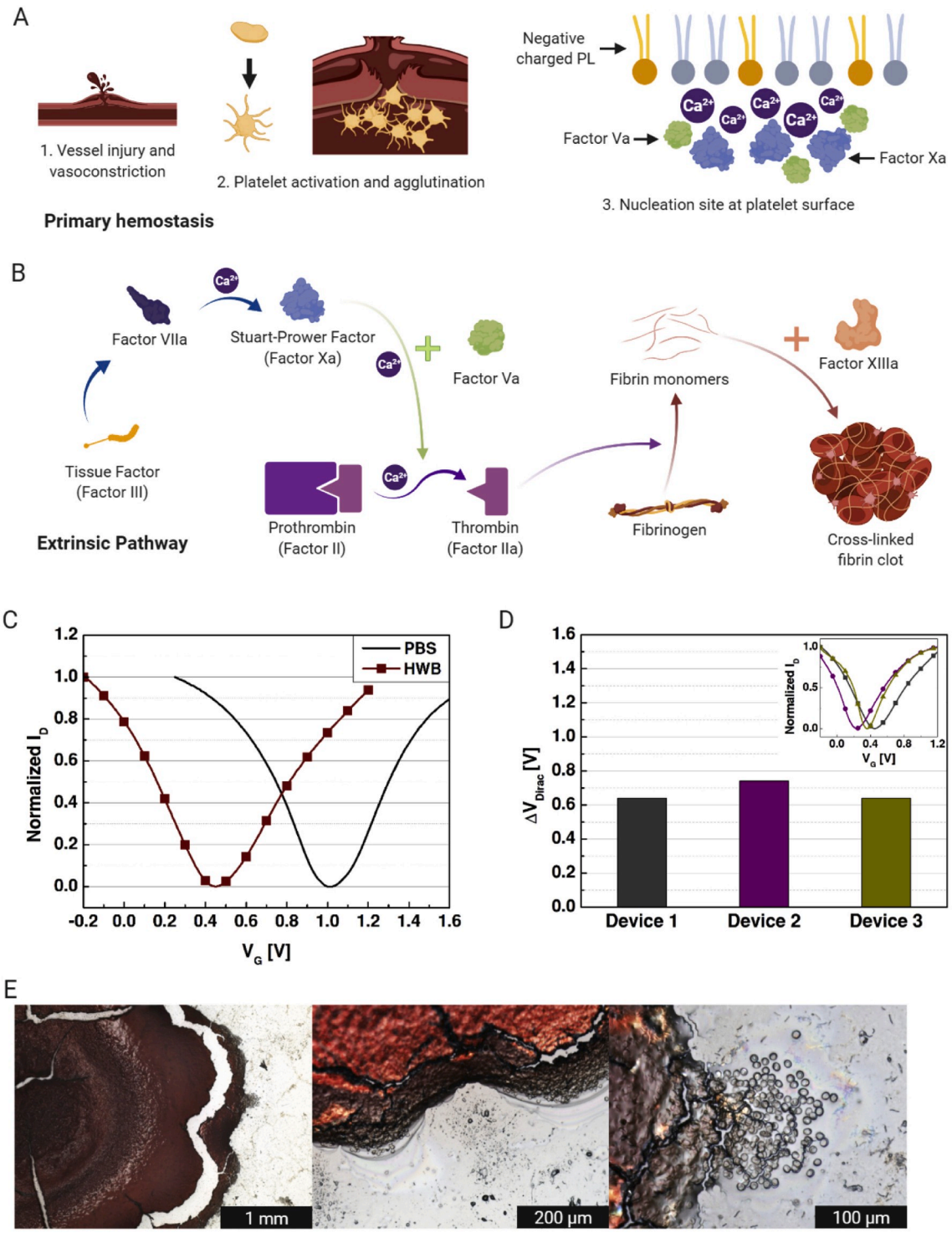

Fig. 3. Hemostasis process and the changes in the charge carrier density over the graphene surface. (A) Primary hemostasis process occurring in the blood sample during the measurements, negatively charged platelet phospholipids are exposed after platelet membrane activation. (B) A brief representation of the extrinsic pathway triggered by the tissue factor to form the fibrin clot. (C) Comparison between HWB sample (initial transfer curve, at 0 min) and PBS solution based on normalized transfer curves from a single device. (D) Shift in the Dirac point voltage values of aliquots of the same sample based on the average reference point (V_{Dirac} = 0.99 V) in three different devices (inset figure shows the transfer curves of each GFET device). (E) Microscope images of a cross-linked fibrin clot, red blood cells, and plasma from the graphene surface transferred onto a bare glass substrate. (For interpretation of the references to colour in this figure legend, the reader is referred to the Web version of this article.)

(Freedman et al., 1996; Morin, 1980). The doping effect decreases when inhibitors (heparin drugs) are added to the blood sample, indicating a slower cascade effect (Fig. 4E). Results from the treated samples show that the most effective activator and inhibitor were the thromboplastin reagent and the parnaparin sodium, respectively. This can be seen when comparing the transfer characteristic curves (Fig. 4F) of both treated samples with the pristine blood.

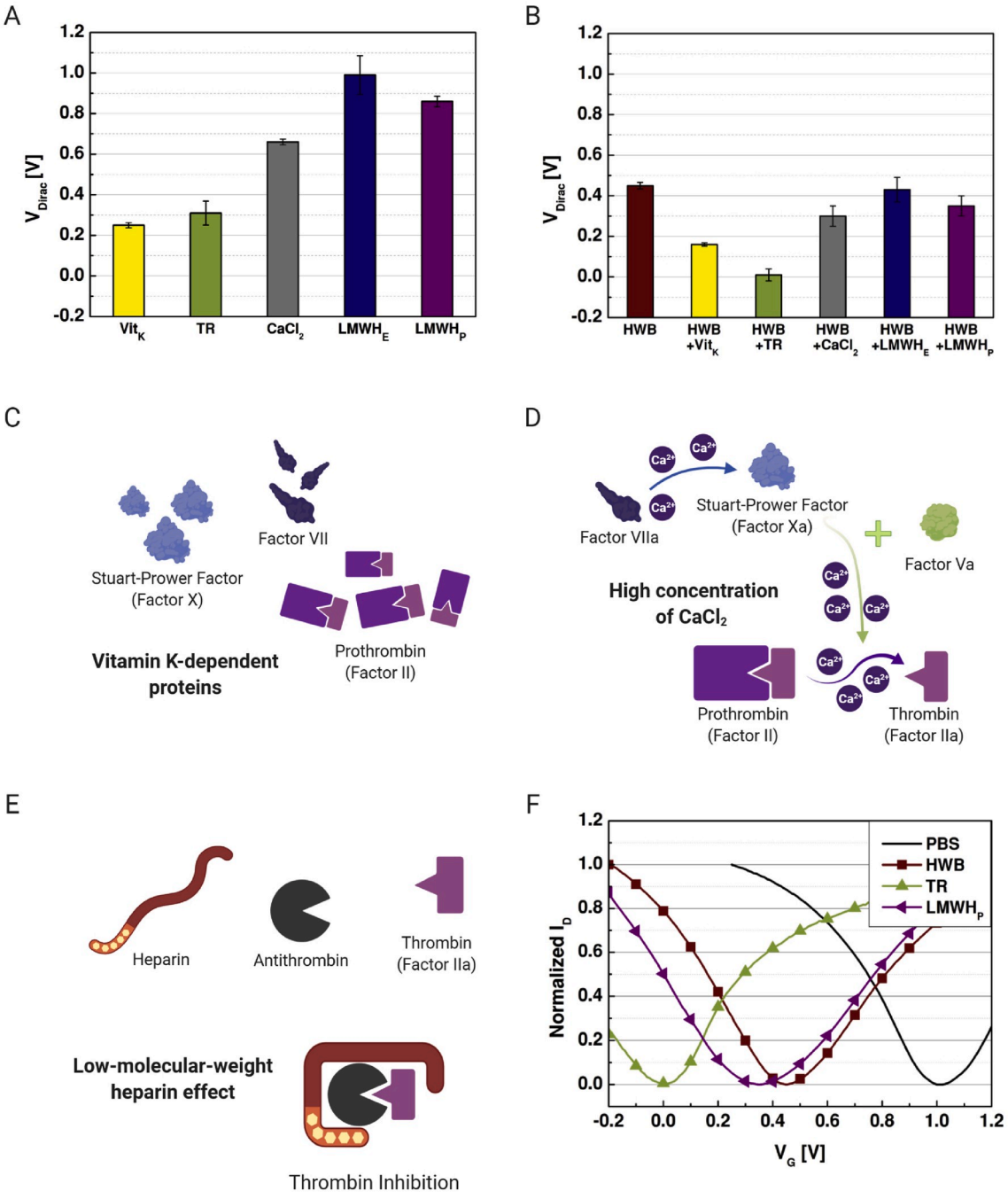

Fig. 4. The effects on the coagulation cascade using GFET devices using different analytes as the electrolyte in GFET device. (A) Dirac point voltage values for different raw analytes. (B) Recorded values of the Dirac point voltage (at 0 min) using pristine and treated blood samples with activators (Vit_K, TR, and $CaCl_2$) and inhibitors ($LMWH_E$ and $LMWH_P$). (C) Presence of vitamin K increases the activity of specific proteins (for example, factor II, factor VII, and factor X). (D) Calcium ions stimulate the binding between the activated factors and the injured site, accelerating the cascade process. (E) Heparin drugs inhibit the thrombin (activated factor II) preventing the clot formation. (F) Comparison between the transfer curves of treated samples with the highest effect on the cascade, the untreated whole blood sample and the buffer solution. Error bars in the bar charts represent the standard deviation of three individual measurements.

3.2. Stabilization of the hemostasis process based on the GFET electrical characteristics

Stabilization of the hemostasis process was verified after injecting 10 μL of recalcified whole blood into the microfluidic channels while the Dirac point voltage values were recorded within a time interval. Human blood samples treated with vitamin K, thromboplastin reagent, $CaCl_2$, and heparin drugs were also used to monitor changes in the neutrality point. I_D-V_G transfer curves were measured every 15 min (Fig. 5A) for 1 h. Using the buffer solution as a reference point, all Dirac point values shifted toward the negative gate voltage when comparing the values at the beginning of the process (at 0 min) with those at the time of total clot formation (at 60 min) (Fig. 5B). The highest shift in V_{Dirac} was observed in the sample treated with the tissue factor (HWB + TR) and is related to the rapid activation of the extrinsic path.

However, the graphene surface began to show stability in the doping effect between 15 and 30 min at which time the variation in the Dirac point voltage was small, indicating a reduction in biochemical interactions due to fibrinolysis (clot dissolution) (Funk, 2012; Ilinskaya and Dobrovolskaia, 2013). This phenomenon was likely caused by the

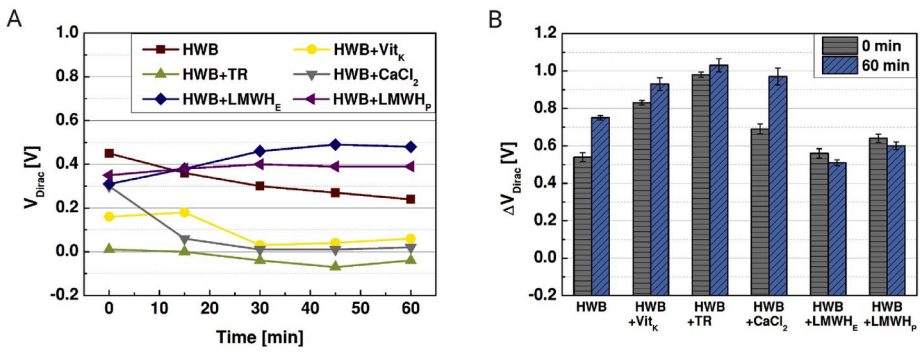

Fig. 5. Stabilization of the hemostasis process based on the Dirac point voltage. (A) Dirac point voltage values for aliquots of the blood samples (10 μL) mixed with 7.5 μL of different activators and inhibitors and measured every 15 min. (B) Shift observed in the Dirac point voltage values from the beginning of the hemostasis process (at 0 min) until the fibrin clot was completely formed (at 60 min) in blood samples mixed with 7.5 μL of activator or inhibitor. Error bars in the bar charts represent the standard deviation of three individual measurements.

action of anticoagulants that inhibit the activators (e.g., vitamin K or positively charged calcium ions) or even by the factors themselves (e.g., activated factor II, also called thrombin) (Funk, 2012; Kuharsky and Fogelson, 2001; Palta et al., 2014). The inhibition of the activated factors and their activators down-regulates cascade activation and consequently, the blood sample on the surface of the graphene begins to show stabilization of the charge carrier concentration (Dahlbäck, 2005; Funk, 2012; Mosnier and Griffin, 2015). The sample treated with activators presented small Dirac point voltage values when compared with other samples, indicating that there were more negative carriers on the graphene surface because of each biochemical reaction in the coagulation cascade. Since the experiment was performed *in vitro*, it was impossible, for example, to regulate fibrinolysis, causing the analyte to present a high and stable concentration of negative charge carriers (remaining activated factors) at the end of the process.

3.3. Monitoring clotting formation using different blood samples

The GFET device performance was evaluated using different blood samples. Following the procedure already described herein, I_D-V_G transfer curves were measured immediately after the blood samples were injected in the devices (Fig. 6A). As expected, there was a gap between the Dirac point voltage values of Sample A (HWB_A) and Sample B (HWB_B). However, both samples showed a reduction in V_{Dirac}, indicating the existence of negative charge carriers on the graphene surface. Dirac point stabilization (Fig. 6B) was observed to occur at different rates for each sample since the level of procoagulants and anticoagulants are different in each human organism which leads to different times over which the coagulation process occurs (Dahlbäck, 2005; Fu et al., 2017; Ilinskaya and Dobrovolskaia, 2013; Palta et al., 2014). Similar behaviour can be observed when the I_D values of the samples from the first 15 min of the coagulation process are plotted (Fig. 6C). The curvature of the line representing the I_D values of Sample A indicates a faster reaction than that representing the I_D values of Sample B.

4. Discussion

The GFET devices were characterized using a buffer solution presenting a Dirac point stability similar to other transistors cited in the literature (Han et al., 2017; Kim et al., 2019; Lei et al., 2017; Reiner-Rozman et al., 2015). The reference neutrality point was around 0.99 V in the GFET devices, while the values reported for other graphene-based devices vary between 0.2 V and 1 V in similar conditions (Cai et al., 2015; Han et al., 2017; Kim et al., 2019; Lei et al., 2017; Reiner-Rozman et al., 2015). In our previous work, we reported an improvement in the technique used to transfer the graphene layer over the substrate surface (Kim et al., 2019). With three layers of PDMS over the CVD-grown graphene, we could guarantee the uniformity after transferring the graphene on the glass substrate and reduce the defects. Then, it was possible to obtain a low standard deviation (SD = ± 0.02 V; n = 40) in the Dirac point voltage values of the GFET devices fabricated for this study. Nevertheless, detection is performed faster when using the GFET device because there is no time required for equilibrium setting due to calibration/immobilization of the active layer surface. Some studies report a long wait time but this stabilization time also depends on the analyte being investigated (Afsahi et al., 2018a; Han et al., 2017; Kim et al., 2019; Reiner-Rozman et al., 2015). For these experiments, there was no need to immobilize the analyte or bioreceptor since a reagent triggered the biochemical reaction directly on the sample. However, when the device is implemented to perform the prothrombin time test, there is a necessity to immobilize the thromboplastin reagent over the graphene surface.

Transfer characteristic curves were measured when the untreated blood was injected into the microchannel. The changes observed in the electrical properties of the whole blood samples subjected to different treatments were used to monitor and evaluate the hemostasis process forming the clot. Then, selectivity was verified using different analytes (activators (vitamin K, thromboplastin reagent, and calcium chloride) and inhibitors (enoxaparin sodium and parnaparin sodium)) as electrolytes. The Dirac point voltage shifted in all experiments, indicating a change in charge carrier concentration on the graphene surface This follows the trends presented in other reports, which showed that a graphene-based transistor is capable of detecting protein, biological serum, and acids (Afsahi et al., 2018b, 2018a; Farid et al., 2015; Lei et al., 2017; Reiner-Rozman et al., 2015) due to the adsorption of the molecules. The n-doping effect observed during the hemostasis process is explained by the complex reactions that occur between the blood-clotting factors, the different plasma proteins, that are activated to form the fibrin clot (Mosnier and Griffin, 2015). The first shift in the Dirac point value was due to platelet activation after the vessel was injured, leading to the exposition of negatively charged phospholipids (Dahlbäck, 2005; Funk, 2012; Harris et al., 2013; Mosnier and Griffin, 2015; Palta et al., 2014). These lipid molecules are necessary for cascade propagation because they bind some of the factors on the platelet membranes attached to the vessel injury (Funk, 2012; Mosnier and Griffin, 2015; Palta et al., 2014). During monitoring, there was no significant variation in the Dirac point voltage between 45 and 60 min, indicating the end of the hemostasis process and therefore the total formation of the clot.

In the devices testing blood samples treated with activators, it was possible to notice the strong effect of vitamin K and thromboplastin reagent in the hemostasis process. Inserting tissue factor into the whole blood sample led to a significant decrease in the Dirac point voltage values and faster fibrin clot formation. However, when using calcium chloride, the initial shift was not large because the ions do not increase or stimulate the activation of other coagulation factors. After 15 min, the Dirac point decreased significantly because calcium ions promote more bindings between the activated factors and the phospholipid site on the platelet surface, thus contributing to the formation of the fibrin clot. When the heparin drugs were included, the behaviour observed in the Dirac point values was as expected because there was no drastic change in values even after the end of the measurement (60 min). These drugs

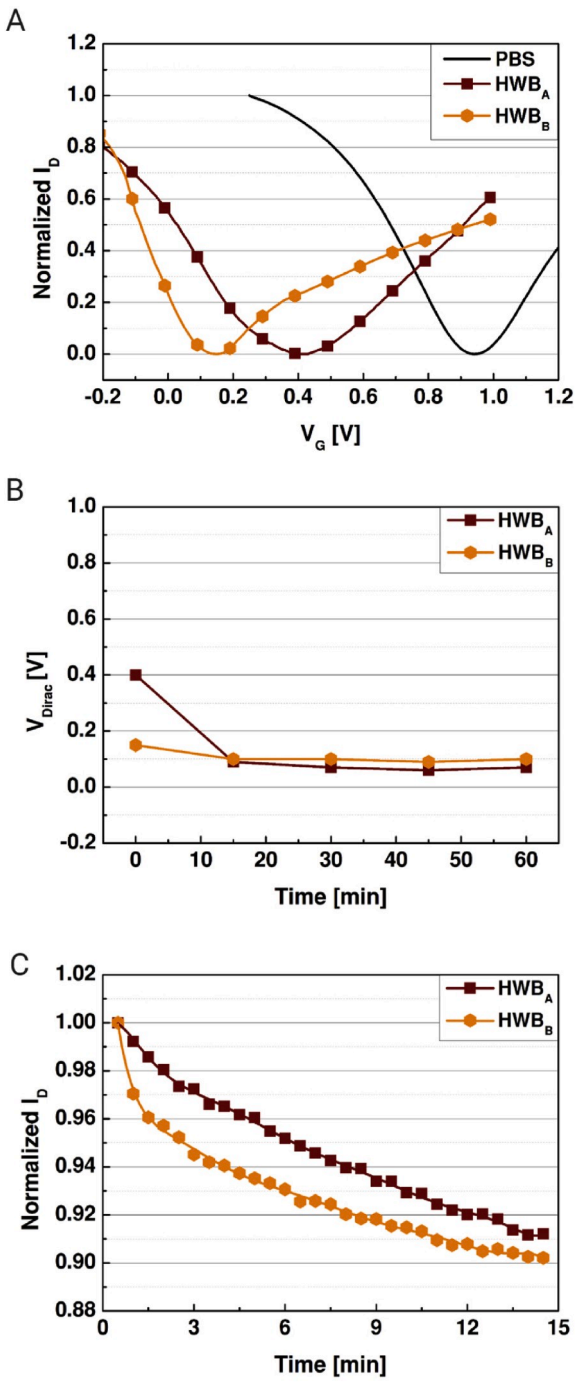

Fig. 6. Investigating the hemostasis process using different blood samples. (A) Normalized transfer characteristic curves of pristine blood samples from different samples. (B) Dirac point voltage recorded at different periods using the pristine samples. (C) Normalized drain current curves presenting divergent behaviors since the level of procoagulants and anticoagulants varies for each human organism.

are responsible for the inhibition of thrombin during the hemostasis process. The parnaparin sodium drug (anti-Xa/anti-IIa ratio $>$ 4) demonstrated a greater effect in restricting such factors than the enoxaparin sodium drug (anti-Xa/anti-IIa ratio = 3.9) because of its higher ratio of anti-Xa to anti-IIa activity (Bugamelli et al., 2008; Schoen et al., 1992).

When studying the device performance with different samples, the transfer characteristic curves exhibited different shapes but the same behaviour in the Dirac point shift for both untreated blood samples. Sample B showed a larger shift, indicating a faster hemostasis reaction than Sample A. This was also observed when evaluating the drain current variation of each sample for 15 min. The curvature slopes indicate that Sample B formed a fibrin clot faster than Sample A. Variations in the biochemical reactions are related to the differences in the concentrations of coagulation components present in the samples from each human organism.

The method proposed in this study was able to monitor the charge concentrations in the blood samples during the hemostasis process using the GFET devices. However, it is necessary to improve the fabrication process and the measurement technique. The materials used to produce the transistors herein have a high cost and are not sustainable and environment-friendly. Additionally, the graphene is easily susceptible to contamination, structural defects, and ambient conditions. Then, it is necessary to improve the transfer method to reduce the defect in the active layer and increase the reproducibility of the experiments. Furthermore, the measurement method needs to be improved to obtain the exact second when occurs the integration between the extrinsic and the common paths based on the current obtained at the point of neutrality. The interval between each transfer curve is around 30 s, but to reproduce and validate the GFET device for PT test, the data should be collected in less than 1 s, since the result of this test should be recorded between 8 and 12 s when the patient presents a normal clot time. For the next plan of this study, the GFET device will be modified and new studies will focus on the PT and the aPTT tests based on the change of the carrier charge concentration in real blood samples in different conditions.

5. Conclusion

In this work, we present a new to a method to evaluate and monitor the hemostasis process based on the measurement of the electrical properties of whole blood samples using a fabricated solution-gate GFET. Small amounts of human blood samples (10 μL) were treated with different biochemicals to alter the hemostasis process by inhibiting or activating the blood factors. Between the selected activators, the thromboplastin reagent affected more the cascade process. However, the heparin drugs presented similar effects when inhibiting the factors based on the shift of the Dirac point voltages. Additionally, different samples were also injected in the devices to verify the reproducibility. Considering that each human organism has different concentrations of the blood factors, the shift in the Dirac point values was also distinctive but presenting the same tendency. The results obtained demonstrate the potential of our solution-gate GFET to investigate the charge concentration of human blood. Also, after the improvement of the fabrication and measurement techniques, the device will be used for point-of-care applications to evaluate different biochemical components that are reacting and interacting during the hemostasis process as a real-time sensor.

Declaration of competing interest

The authors declare that they have no known competing financial interests or personal relationships that could have appeared to influence the work reported in this paper.

CRediT authorship contribution statement

Ariadna Schuck: Conceptualization, Methodology, Investigation, Software, Formal analysis, Writing - original draft, Writing - review & editing. **Hyo Eun Kim:** Methodology, Writing - review & editing. **Kyung-Mo Jung:** Investigation. **Willyan Hasenkamp:** Writing - review & editing. **Yong-Sang Kim:** Writing - review & editing, Supervision, Funding acquisition.

Acknowledgements

This work was supported in part by the National Research Foundation of Korea (NRF) grant funded by the Korea government (No. NRF-2018R1D1A1B05049787), and by the Loyola Fund for Academic Support (Programa Fundo Loyola de Apoio Acadêmico) Scholarship from the Universidade do Vale do Rio dos Sinos (UNISINOS). The authors would like to recognize Dra. Priscila Schmidt Lora and Júlia Konzen Moreira from UNISINOS for their valuable technical suggestions and input. The authors would also like to thank Mauricio Gammertt Rohnelt from itt Fuse for the microscope images (Automated Digital Microscope ZEISS Smartzoom 5).

Appendix A. Supplementary data

Supplementary data to this article can be found online at https://doi.org/10.1016/j.bios.2020.112167.

References

Afsahi, S., Lerner, M.B., Goldstein, J.M., Lee, J., Tang, X., Bagarozzi, D.A., Pan, D., Locascio, L., Walker, A., Barron, F., Goldsmith, B.R., 2018a. Biosens. Bioelectron. 100, 85–88.
Afsahi, S., Lerner, M.B., Goldstein, J.M., Lee, J., Tang, X., Bagarozzi, D.A., Pan, D., Locascio, L., Walker, A., Barron, F., Goldsmith, B.R., 2018b. Biosens. Bioelectron. 100, 85–88.
Andronescu, C., Schuhmann, W., 2017. Curr. Opin. Electrochem. 3.
Bazaev, I.A., Przhiyalgovskaya, A.V., Rudenko, P.A., Tronin, A.V., Lifshits, G.I., 2015. Biomed. Eng. 49, 136–141.
Bermingham, M.A.C., Boggust, W.A., O'Meara, R.A.Q., 1968. Nature 218, 695–696.
Bhagavan, N.V., 2002. Biochemistry of hemostasis. In: Medical Biochemistry. Elsevier, pp. 839–872i.
Boon, G.D., 1993. Toxicol. Pathol. 21, 170–179.
Bugamelli, S., Zangheri, E., Montebugnoli, M., Guerra, L., 2008. Vasc. Health Risk Manag. 4, 983–990.
Cai, B., Huang, L., Zhang, H., Sun, Z., Zhang, Z., Zhang, G.-J., 2015. Biosens. Bioelectron. 74, 329–334.
Cakmak, O., Kilinc, N., Ermek, E., Mostafazadeh, A., Elbuken, C., Yaralioglu, G.G., Urey, H., 2014. LoC sensor array platform for real-time coagulation measurements. In: 2014 IEEE 27th International Conference on Micro Electro Mechanical Systems (MEMS). IEEE, pp. 330–333.
Chapin, J.C., Hajjar, K.A., 2015. Blood Rev. 29, 17–24.
Cheng, Tzong-Jih, Chang, Hsein-Chang, Lin, Tsun-Mei, 1998. Biosens. Bioelectron. 13, 147–156.
Dahlbäck, B., 2005. J. Intern. Med. 257, 209–223.
Dong, X., Shi, Y., Huang, W., Chen, P., Li, L.-J., 2010. Adv. Mater. 22, 1649–1653.
Farid, S., Meshik, X., Choi, M., Mukherjee, S., Lan, Y., Parikh, D., Poduri, S., Baterdene, U., Huang, C.-E., Wang, Y.Y., Burke, P., Dutta, M., Stroscio, M.A., 2015. Biosens. Bioelectron. 71, 294–299.
Freedman, S.J., Blostein, M.D., Baleja, J.D., Jacobs, M., Furie, B.C., Furie, B., 1996. J. Biol. Chem. 271, 16227–16236.
Fu, W., Feng, L., Panaitov, G., Kireev, D., Mayer, D., Offenhäusser, A., Krause, H.-J., 2017. Sci. Adv. 3, e1701247.
Funk, D.M.A., 2012. Hematol. Am. Soc. Hematol. Educ. Progr. 460–465, 2012.
Golder, M., Mewburn, J., Lillicrap, D., 2013. Thromb. Haemostasis 109, 53–60.
Han, D., Chand, R., Kim, Y.S., 2017. Biosens. Bioelectron. 93, 220–225.
Harris, L.F., Castro-López, V., Killard, A.J., 2013. TrAC Trends Anal. Chem. (Reference Ed.) 50, 85–95.
Ilinskaya, A.N., Dobrovolskaia, M.A., 2013. Nanomedicine 8, 969–981.
Kim, H.E., Schuck, A., Lee, J.H., Kim, Y.-S., 2019. Sensor. Actuator. B Chem.
Kuharsky, A.L., Fogelson, A.L., 2001. Biophys. J. 80, 1050–1074.
Kwak, Y.H., Choi, D.S., Kim, Y.N., Kim, H., Yoon, D.H., Ahn, S.-S., Yang, J.-W., Yang, W. S., Seo, S., 2012. Biosens. Bioelectron. 37, 82–87.
Lane, D.A., 2005. Blood 106, 2605–2612.
Lei, K.F., Chen, K.-H., Tsui, P.-H., Tsang, N.-M., 2013. PLoS One 8, 1–7.
Lei, Y.-M., Xiao, M.-M., Li, Y.-T., Xu, L., Zhang, H., Zhang, Z.-Y., Zhang, G.-J., 2017. Biosens. Bioelectron. 91, 1–7.
Levesque, P.L., Sabri, S.S., Aguirre, C.M., Guillemette, J., Siaj, M., Desjardins, P., Szkopek, T., Martel, R., 2011. Nano Lett. 11, 132–137.
Maji, D., Suster, M.A., Stavrou, E., Gurkan, U.A., Mohseni, P., 2015. Monitoring time course of human whole blood coagulation using a microfluidic dielectric sensor with a 3D capacitive structure. In: 2015 37th Annual International Conference of the IEEE Engineering in Medicine and Biology Society (EMBC), pp. 5904–5907.
Maji, D., Suster, M.A., Kucukal, E., Sekhon, U.D.S., Gupta, A.S., Gurkan, U.A., Stavrou, E. X., Mohseni, P., 2017. IEEE Trans. Biomed. Circuits Syst. 11, 1459–1469.
Mao, S., Chen, J., 2017. J. Mater. Res. 32, 2954–2965.
Merli, G.J., Groce, J.B., 2010. P T 35, 95–105.
Morin, R.J., 1980. Ann. Clin. Lab. Sci. 10, 463–473.
Mosnier, L.O., Griffin, J.H., 2015. Control of coagulation reactions. In: Kaushansky, K., Lichtman, M.A., Prchal, J.T., Levi, M.M., Press, O.W., Burns, L.J., Caligiuri, M. (Eds.), Williams Hematology, 9e. McGraw-Hill Education, New York, NY.
Müller, L., Sinn, S., Drechsel, H., Ziegler, C., Wendel, H.P., Northoff, H., Gehring, F.K., 2010. Anal. Chem. 82, 658–663.
Palta, S., Saroa, R., Palta, A., 2014. Indian J. Anaesth. 58, 515–523.
Periayah, M.H., Halim, A.S., Mat Saad, A.Z., 2017. Int. J. Hematol. stem cell Res. 11, 319–327.
Ramaswamy, B., Yeh, Y.T.T., Zheng, S.Y., 2013. Sensors Actuators, B Chem. 180, 21–27.
Reiner-Rozman, C., Larisika, M., Nowak, C., Knoll, W., 2015. Biosens. Bioelectron. 70, 21–27.
Forsyth, Rhiannan, Devadoss, Anitha, Guy, Owen, 2017. Diagnostics 7, 45.
Schoen, P., Lindhoux, T., Hemker, H.C., 1992. Br. J. Haematol. 81, 255–262.
Sperling, C., Maitz, M.F., Grasso, S., Werner, C., Kanse, S.M., 2017. ACS Appl. Mater. Interfaces 9, 40107–40116.
Suvarnaphaet, P., Pechprasarn, S., 2017. Sensors 17, 2161.
Tormoen, G.W., Khader, A., Gruber, A., McCarty, O.J.T., 2013. Phys. Biol. 10, 036003.
Tran, T.T., Mulchandani, A., 2016. TrAC Trends Anal. Chem. (Reference Ed.) 79, 222–232.
Tripodi, A., 2016. Clin. Chem. 62, 699–707.
Wahed, A., Dasgupta, A., 2015. Chapter 15 - essentials of coagulation. In: Wahed, A., Dasgupta, A. (Eds.), Hematology and Coagulation. Elsevier, San Diego, pp. 231–261.
White, R.H., Ginsberg, J.S., 2003. Br. J. Haematol. 121, 12–20.
Winter, W.E., Flax, S.D., Harris, N.S., 2017. Lab. Med. 48, 295–313.
Yang, C.-L., 2013. J. Med. Biol. Eng. 33, 319.
Yao, C., Qu, L., Fu, W., 2013. Sensors 13, 6946–6956.